Functionalized Iron Hydroxyapatite as Eco-friendly Catalyst for NH3-SCR Reaction: Activity and Role of Iron Speciation on the Surface

S. Campisi, M. Galloni, S. G. Marchetti, A. Auroux, G. Postole, A. Gervasini

10.1002/cctc.201901813

Functionalized iron hydroxyapatite as ecofriendly catalyst for NH_3-SCR reaction: activity and role of iron speciation on the surface

S. Campisi,[a] M.G. Galloni,[a] S.G. Marchetti,[b] A. Auroux,[c] G. Postole,[c] and A. Gervasini*[a]

[a] *Dipartimento di Chimica, Università degli Studi di Milano, via Camillo Golgi 19, 20133 Milano, Italy. E-mail:* antonella.gervasini@unimi.it (corresponding author)

[b] *Centro de Investigación y Desarrollo en Procesos Catalíticos, CINDECA (UNLP-CONICET), Calle 47 Nº. 257, C.P. 1900, La Plata, Argentina*

[c] Univ Lyon, Université Claude Bernard Lyon 1, CNRS, IRCELYON, F-69626, Villeurbanne, France.

Electronic supplementary information (ESI) available.

10.1002/cctc.201901813

Abstract

Eco-friendly catalysts have been obtained by functionalizing hydroxyapatite (HAP) with iron (Fe/HAP), according to three preparative methods (*flash* ionic exchange, deposition-precipitation, and impregnation). Fe/HAP samples (*ca.* 2-7 wt.% Fe) have been tested in the reaction of NO_x reduction by ammonia (NH_3-SCR) in the 120-500°C interval with different NH_3/NO ratios (0.6-2) at fixed contact time (0.12 s). All Fe/HAP samples were active and selective in the NH_3-SCR reaction starting from *ca*. 350°C. Better performances have been observed on catalysts prepared by deposition-precipitation and impregnation (about 70% of NO_x conversion and selectivity to N_2 higher than 95% at 350°C), where α-Fe_2O_3 and *3D*-Fe_2O_3 nanoclusters were present, as indicated by Mössbauer and UV-Vis-DR spectroscopies. On the opposite, paramagnetic Fe^{3+} centers were the predominant species on samples prepared by *flash* ionic exchange. Further characterisation techniques (XRPD, N_2-physisorption, acidity by NH_3 adsorption, and H_2-TPR) have concurred to elucidate Fe-sitting HAP and structure-activity relationships.

Keywords

Iron hydroxyapatite; Catalyst preparation; Environmental chemistry; Denitrification; Moessbauer spectroscopy.

Introduction

Nowadays, catalytic technologies represent the most effective and common solution to environmental issues related to air, water, and soil pollution. Although catalysis can be considered a well consolidated field, the need to meet ever more stringent criteria of sustainability and efficiency requires a continuous effort to improve and optimize the current catalytic processes and related catalytic materials [1]. Actually, the development of high performance, non toxic, low-cost and eco-friendly materials to be used as catalysts is a key factor for the achievement of a sustainability-driven environmental catalysis.

Selective catalytic reduction by ammonia (NH_3-SCR) is the most commonly used process for the abatement of nitrogen oxides (NO_x), which are considered major pollutants in air [2]. Some reactions starting from NO or NO_2 can occur according to the following equations (Eqs. 1-4):

$$4NO + 4NH_3 + O_2 \rightarrow 4N_2 + 6H_2O \quad \textit{“standard SCR”} \qquad (1)$$

$$6NO + 4NH_3 \rightarrow 5N_2 + 6H_2O \quad \textit{“slow SCR”} \qquad (2)$$

$$6NO_2 + 8NH_3 \rightarrow 7N_2 + 12H_2O \quad \textit{“NO}_2\textit{ SCR”} \qquad (3)$$

$$NO + NO_2 + 2NH_3 \rightarrow 2N_2 + 3H_2O \quad \textit{“fast SCR”} \qquad (4)$$

Despite the industrial and commercial success of NH_3-SCR process, this process is undergoing a constant evolution aimed to satisfy the stringent standards for NO_x emission [3].

Several materials have been proposed, studied, and successfully employed as catalysts in the NH_3-SCR reaction over the years. In the last decades, the use of metal exchanged zeolites as SCR catalysts has become widespread. However, the expensiveness of zeolite synthesis as well as some practical lacks of zeolite-based catalysts (e.g. poor hydrothermal stability, low resistance to sulfur poisoning) constitute no-negligible limitations of these systems and an unequivocal stimulus to develop valid alternatives.

Recent studies [4-7] have demonstrated that the deposition of transition metal species (e.g. Ag, Cu, Fe) onto calcium hydroxyapatite results in effective catalysts for NH_3-SCR reaction.

Stoichiometric calcium hydroxyapatite (HAP, chemical formula $Ca_{10}(PO_4)_6(OH)_2$) is an inorganic compound that can be found in nature as mineral or main inorganic component of mammal bones. HAP crystal lattice is characterized by a hexagonal symmetry (space group $P6_3/m$) assured by a three-dimensional framework of hexagonally packed tetrahedral PO_4^{3-} ions. Ca^{2+} ions are located in two non-equivalent crystallographic sites, Ca(1) and Ca(2) sites, which are characterized by a different coordination number (9 and 7, respectively) and environment [8]. The high mobility of Ca^{2+} ions and the high coordination number of both Ca sites allow their substitution in both Ca(1) and Ca(2) positions by several cations, many of them of catalytic interest. In addition, many anions can replace either OH^- or PO_4^{3-} ions or both [9]. This intrinsic capability to exchange the framework ions and allocate other metal species, similarly to zeolites, together with the amphoteric character of HAP surfaces allow obtaining interesting functionalized materials, which are experiencing a growing success in heterogeneous catalysis [7, 10-12].

Actually, copper-hydroxyapatites (Cu/HAP) have exhibited remarkable performances in terms of activity, selectivity and durability when tested as catalysts in NH_3-SCR reaction [7, 11]. The copper precursors as well as the deposition procedure affect the copper speciation onto the hydroxyapatite surfaces and the catalytic performance of Cu/HAP in NH_3-SCR, as demonstrated by Gervasini et al. [11]. It was found that the Cu/HAP catalysts prepared starting from copper nitrate, as precursor, could be associated with the best active and selective SCR catalysts. In addition, an optimum Cu-concentration on HAP of *ca*. 6 wt.% was observed independently of the used Cu-deposition method.

A recent comparative study between copper- and iron-modified HAP catalysts prepared by ion exchange procedure [13] revealed that both catalyst series were active and selective for NH_3-SCR reaction, even if in different operating temperature intervals. This evidence has important practical implications, allowing to select the proper catalyst according to the flue gas temperature window. In any case, iron-based catalysts were in general less active than Cu/HAP, even if they maintained good activity in a broader operating temperature range. Iron-catalysts are less studied than the relevant copper catalysts for the NH_3-SCR process; due to their low cost, they could have high potentiality for

application, if suitably developed. It is known that the control of metal sitting, speciation, and nuclearity, represents a key step for the attainment of catalysts with enhanced activity. Accordingly, a deeper understanding of the factors influencing iron nuclearity and their sitting on HAP surface and the impact of these on the catalytic performances is required.

In this work, calcium hydroxyapatite has been functionalized with iron in different amount (ca. 2-7 wt.%) from iron(III) nitrate, as precursor, according to three preparative methods (*flash* ionic exchange, deposition-precipitation and wetness impregnation). Depending on the specific experimental conditions, the added iron centers could be allocated as isolated species in two different sites with different coordination environment (Ca(1) and Ca(2)), or alternatively undergo surface agglomeration with formation of Fe-aggregates of different size. A suite of characterization techniques (Mössbauer and UV-Vis spectroscopies, XRPD, N_2-physisorption, acidity by NH_3 adsorption, and H_2-TPR) was also used to investigate on iron speciation and sitting on HAP and to deduce relevant structure-activity relationships.

Experimental section

Material used and catalyst preparation

Hydroxyapatite used (AV15012 lot) was kindly supplied by Solvay, Belgium (Soda Ash & Derivatives Department); its preparation procedure, composition and main properties are detailed in Ref. [14]. As-obtained hydroxyapatite sample was thermally treated at 500°C for 1 h with controlled temperature rate (1°C/min) before any successive treatment.

The functionalized hydroxyapatite samples with different iron-loading (in the range 2-7 wt.%) were prepared by depositing Fe(III) nitrate on hydroxyapatite surface with three different procedures: *i*) a modified ionic exchange procedure, named *flash* ionic exchange; *ii*) deposition-precipitation; and *iii*) incipient wetness impregnation. For each preparation, HAP in powder, previously dried at 120°C overnight, was used; the detailed procedures of each type of preparation are below reported.

Flash ionic exchange

Three samples (with iron loading in the range 2-7 wt.%) were prepared by *flash* ionic exchange procedure, a modified procedure compared to the conventional one, specially developed to obtain well dispersed and isolated Fe^{3+} centres on the hydroxyapatite surface, starting from an aqueous solution of a Fe-salt precursor.

For each preparation, 250 mL of iron(III) nitrate ($Fe(NO_3)_3 \cdot 9H_2O$) solution (concentration range from 0.005 to 0.035 M) were first thermostatted at 40°C. To avoid the precipitation of iron(III) hydroxide, the pH was adjusted to value of *ca*. 3 by HNO_3 addition. Weighed amount of HAP powder (typically *ca.* 6 g) was added to the iron(III) nitrate solution and the suspension was kept under stirring for 15 minutes. This short time guarantees both preserving surface and structural properties of HAP, which is known to be sensitive to amorphization and it can dissolve under acidic condition [15], and hindering self-agglomeration of Fe^{3+} species. The obtained pale yellow samples were filtered, washed with deionized water, and dried at 120°C overnight, finally calcined at 500°C for 1 h at controlled rate ($1°C \cdot min^{-1}$) under static air. The collected samples were labelled as FeX/HAP_{IE}, where X is the nominal Fe loading, in wt.%.

Deposition-precipitation

Two samples (with iron loading of 5 and 7 wt.%) were prepared by deposition-precipitation procedure.

For each preparation, 250 mL of iron(III) nitrate ($Fe(NO_3)_3 \cdot 9H_2O$) solution (concentration range 0.0226 M or 0.0324 M) were prepared at room temperature (r.t.); the pH of solution was adjusted to the value of *ca*. 3 by HNO_3 addition to prevent the precipitation of iron(III) hydroxide. The sample preparation was carried out in a four necked flask, provided with thermometer and reflux condenser; 100 mL of 0.2M NaOH solution were put in the flask and thermostatted at 40°C under stirring (250 rpm). A given amount of HAP powder (typically *ca*. 6 g) was introduced to NaOH solution before the addition of the previously prepared solution of iron(III) nitrate by a syringe pump with regular

flow rate (1 mL·min^{-1}). The suspension was maintained under stirring till complete addition of iron-solution, while the pH of the solution was maintained to values of 9 - 11 by addition of small quantities of NaOH solution (0.2 M). The precipitate was filtered and thoroughly washed with deionized water to remove the excess of sodium hydroxide. The obtained brown sample was dried at 120°C overnight and calcined at 500°C for 1 h at controlled rate (1°C·min^{-1}) under static air. The collected samples were labelled as FeX/HAP$_{DP}$, where X is the nominal Fe loading, in wt.%.

Incipient wetness impregnation

Two samples (with iron loading of 5 and 7 wt.%) were prepared by incipient wetness impregnation procedure.

For each preparation, 10 mL of $Fe(NO_3)_3 \cdot 9H_2O$ solution (concentration range 0.565 M or 0.809 M) were prepared; the pH of solution was maintained at value of *ca*. 5 by HNO_3 addition. A weighted amount of HAP powder (typically *ca*. 6 g) was put in a necked flask and connected to a Büchi rotary evaporator, maintained at 80°C. The Fe impregnation was performed by adding the iron (III) solution dropwise to HAP, using a dropping funnel connected to the rotary evaporator and alternating cycles of dropping of the Fe-solution and solvent evaporation. The addition of iron solution to HAP powder lasted a total of 4-5 h. The obtained brown sample was dried at 120°C overnight and calcined at 500°C for 1 h at controlled rate (1°C·min^{-1}) under static air.

The prepared samples were labelled as FeX/HAP$_{WI}$, where X is the nominal Fe loading, in wt.%. The Fe-loading corresponded to the known amount of iron added to HAP. Evident differences in the colour of Fe/HAP powders emerged depending on the preparation route (Fig. S1): the colour varied from pale yellow (for the series prepared by *flash* ionic exchange) to brown (for the samples prepared by wetness impregnation and deposition precipitation methods).

The Fe loading of the sample series prepared by *flash* ionic exchange and deposition-precipitation was double-checked by atomic absorption spectroscopic (AAS) analysis on the solid, after mineralization of a small amount (*ca.* 50 mg) of sample, and on the residual iron(III) nitrate solution, after separation of solid by filtration.

Catalyst characterisation

X-ray powder diffraction (XRPD) spectra were collected with a Philips PW 3020 powder diffractometer, fitted with PW 1830 generator and copper tube (CuK_{α}=1.54060 Å) and equipped with X-ray source operating at 40 kV and 25 mA. Powder diffractograms were collected by continuous scan in the 2θ range from 10° to 60°, step size of 0.05° 2θ, time for step of 5 sec, scan speed of 0.010 $2\theta \cdot s^{-1}$, number of steps of 1000, and total time of 1h 23 min.

Specific surface area (S.S.A.), pore volume, and pore size distribution of the samples were determined by adsorption and desorption isotherms of N_2 (99.9995% purity) at −196°C by using an automatic analyzer of surface area (Sorptomatic 1990 version instrument from Thermo Scientific Carlo Erba). The samples (*ca*. 0.2 g sieved as particles in the range of 80-200 mesh) were outgassed at 350°C for 4 h under vacuum, in order to remove water and other volatile organic compounds adsorbed on the surface. The specific surface area values were computed using *3-parameters* BET (Brunauer-Emmet-Teller) equation. The pore volume and pore size distribution were determined by using BJH (Barrett-Joyner-Halenda) method.

Mass loss of bare and Fe-loaded hydroxyapatite samples was determined by thermogravimetric analysis (TGA 7, Perkin Elmer analyzer). Prior to the analysis, the samples were dried at 120°C overnight and a weighted amount (*ca*. 10-15 mg) was loaded on the pan of the thermobalance. Each experiment was carried out under air flowing gas (30 $mL \cdot min^{-1}$) with the following method: *i)* isothermal step at 35°C for 5 min; *ii)* heating from 35 to 500°C at $10°C \cdot min^{-1}$; *iii)* isothermal step at 500°C for 60 min; and *iv)* cooling to 40°C.

Acidity of both bare hydroxyapatite and Fe loaded catalysts was evaluated by NH_3 probe adsorption by flowing dynamic experiments. The sample, previously pressed, crushed, and sieved to obtain particles in the range 45-60 mesh, was dried and weighed (*ca*. 0.20 g). It was then put on a porous septum in a quartz reactor and maintained at 120°C for 30 min under flowing air; then, it was contacted with a NH_3/He mixture flow (6 $NL \cdot h^{-1}$) at NH_3 concentration of ca. 500 ppm. The NH_3

concentration vented by the reactor was continuously monitored by an online FT-IR spectrophotometer (Bio-Rad, DTGS detector equipped with a multiple reflection gas cell, path length 2.4 m) at 966 cm^{-1}. On each sample, NH_3 was completely adsorbed for a given measured time, as observed from the trace of the NH_3 line at 966 cm^{-1}, that was recorded as a function of time. When the saturation of the acid sites under the flowing NH_3 concentration was attained, the NH_3 signal restored at level corresponding to its concentration in the starting mixture. From the evaluation of the time during which the NH_3-signal remained to zero, the amount of acid sites has been evaluated, as reported in Eq.5:

$$\frac{\mu moles_{NH3\,(ads)}}{g_{sample}} = \frac{[NH_3]_{fed} \cdot F \cdot t \cdot P}{RT \cdot m_{sample}} \quad (5)$$

where $[NH_3]_{fed}$ is the flowing NH_3 concentration (ppm); F is the total flow rate of NH_3/He mixture (in $NL \cdot h^{-1}$); t is the time during which NH_3 was completely adsorbed (in min); P is the pressure (in atm) and m_{sample} is the mass of the sample (in g).

Assuming a 1:1 stoichiometry for the NH_3 adsorption on the surface acid site, the amount of acid sites *per* sample mass or *per* surface unit (in $\mu equiv \cdot g^{-1}$ or $\mu equiv \cdot m^{-2}$) was evaluated. Measurements were replicated and in all cases a percent relative uncertainty of less than 3% was obtained.

Reduction analyses in programmed temperature (H_2-TPR) were realized on fresh Fe/HAP samples. A TPDRO–1100 (from Thermo Scientific) equipped with a thermal conductivity detector (TCD), a quartz reactor, and a filter filled with soda lime for trapping acid gases and water was employed. TPR measurement was carried out using H_2/Ar (5.00% v/v) as reducing gas mixture. The gas flow rate was adjusted by mass flow controllers to 20 $cm^3 \cdot min^{-1}$. The obtained TPR peaks were integrated for quantitative determination of H_2 consumed; calibrations were performed with CuO bulk as reference material. TPR runs were carried out by a heating step from r.t. to 900°C, at rate of $10°C \cdot min^{-1}$. Dried sample mass in powder (*ca*. 0.07-0.2 g, equivalent to about 35-45 μmol of Fe_2O_3) was used, this allowed to maintain the values of the sensitivity and resolution parameters [16-17] around 120 s and 20°C, respectively, for all the analyses.

The experimental H_2-TPR curves obtained have been decomposed with the Software OriginPro8 by using combinations of Gaussian functions.

Spectroscopic characterization

Mössbauer spectra were obtained in transmission geometry with a 512-channel constant acceleration spectrometer (WissEl, Germany), using a source of ^{57}Co in Rh matrix of nominally 50 mCi. The sample ideal thickness was evaluated considering the weight percentages of the different elements of each catalyst (about 100 mg of powder were used for a holder of 1.8 cm of diameter). Velocity calibration was performed using a 12-μm-thick α-Fe foil as reference. Spectra were collected at -260 and 25°C. Measurements at low temperatures were done working with a closed-cycle cryogenic system (ARS, Model DE-202, USA). Each spectrum was folded to minimize geometric effects and the experimental data were fitted using a commercial program with constraints named Recoil [18].

DC magnetization (M) as a function of applied magnetic field (H) was obtained at room temperature using vibrating sample magnetometer (VSM) from LakeShore 7404 (maximum applied field H_{max} = 20000 Oe). The sample (37 mg, dry powder) was located inside a gel capsule and pressed in order to avoid displacements during the measurement.

UV-Vis diffuse reflectance spectra of catalyst powders were recorded with a double beam UV-Vis-NIR scanning spectrophotometer (Shimadzu, UV-3600 Plus, Japan) equipped with an integrating sphere (ISR-603) at room temperature in the wavelength region 200-1200 nm. Ultrafine barium sulphate was used as reference material. A given amount of dried powder (120°C overnight) was finely ground, uniformly pressed in a circular disk (E.D. about 4 cm) and put in the sample-holder. The latter was inserted in a quartz cuvette and put on a window of the integrating sphere for reflectance measurements. The measured reflectance spectra (R_∞%) were converted to absorbance (Abs) according to Eq. 6:

$$Abs = - \log (R_\infty\%/100) \quad (6)$$

The collected UV-Vis-DR spectra (Absorbance vs. wavelength, nm) in the range 200-800 nm have been decomposed with the Software OriginPro8 by using a combination of Gaussian functions.

Catalytic testing of NO_x reduction with ammonia (NH_3-SCR)

Catalytic performances of iron loaded catalysts in NH_3-SCR reaction were evaluated by using a continuous laboratory-reaction line equipped with a set of mass flow controllers (Bronkhorst, Hi-Tec and Brooks Instruments), a tubular vertical electric oven (Eurotherm Controller-Programmer type 818), a glass tubular catalytic micro reactor (5 mm i.d.), and an on line FT-IR spectrophotometer (Bio-Rad, DTGS detector) for qualitative and quantitative determination of the fed and vented gaseous species.

For each experiment, the catalyst samples (about 0.20 g), previously pressed, crushed and sieved so as to obtain particles in the range 45-60 mesh, were dried at 120°C overnight. Then, they were pre-treated in situ under O_2/N_2 flow (20% v/v) at 120°C for 30 min. The catalyst activity was studied as a function of the temperature (120-500°C), maintaining constant the concentration of feeding gas mixture and with a total flow rate of 6 $NL \cdot h^{-1}$ (corresponding to contact time of 0.12 s). Each temperature was maintained for 60 min in order to allow the attainment of the steady-state condition. The temperature was increased at step ramping the temperature at $10°C \cdot min^{-1}$. The fed mixture was prepared mixing about 500 ppm of NO, 500 ppm of NH_3 and about 10,000 ppm of O_2 in nitrogen. After the mixing, the effective fed mixture contained also NO_2 (about 50 ppm of NO_2). The gas-mixture flowed through the catalyst particles at 120°C until the catalyst surface was saturated with NH_3.

Additional NH_3-SCR catalytic tests were also performed by varying the fed NH_3 concentration (from 300 to 1000 ppm) at fixed NO concentration (500 ppm) in the same temperature range and contact time (0.12 s).

The gaseous stream vented from the reactor was monitored by a FT-IR equipped with a multiple reflection gas cell (with 2.4 m path length; resolution of 2 cm^{-1}; sensibility of 1.5 and 92 scans per

180 seconds) for quantifying the unconverted reagents and/or reaction products. The total absorbance of all the IR active species (Gram–Schmidt profile) flowing from the reactor was continuously recorded as a function of time, while the reaction temperature was changing.

The NO, NO_2, and NH_3 and other formed species (if any) were quantified from the peak height of a selected absorbance line, taking into account the measured calibration factors. N_2 concentration was determined from the difference between the fed NH_3 and NO_x (NO plus NO_2) concentrations and the sum of the unreacted NH_3 plus $NO+N_2O+NO_2$ concentrations, eventually formed. Computational details can be found in Supplementary Material (Table S1).

Results and Discussion

Fe/HAP samples and properties

Bare calcium hydroxyapatite, used as support for Fe/HAP catalysts, was characterized after calcination at 500°C in order to remove water and any other impurities and to stabilize its structure. Thermally treated HAP is a mesoporous solid with a specific surface area of 53 $m^2 \cdot g^{-1}$ and a pore size distribution centred at ca. 8 nm (Table 1). The experimental diffractogram of calcined HAP obtained from XRPD analysis contained all the characteristic features of the HAP reference pattern from ICDD PDF database (JCPDS 00-009-0432), thus confirming the crystallinity of the material.

Hydroxyapatite has been functionalized with different amount of iron (from 2 to 7 wt.%) introduced with three different methods: *flash* ionic exchange, deposition-precipitation, and wetness impregnation.

In the first method, the well known Ca^{2+} exchange ability of HAP has been exploited for preparing three samples containing different concentration of dispersed Fe^{3+} species with homogeneous distribution at the HAP surface. The Fe-concentration of the three Fe/HAP catalysts, as determined by ICP analysis on the digested samples, are reported in Table 1. The lower or higher amount of iron of the samples did not cause any structural modification. XRP-diffractions of bare HAP and Fe/HAP_{IE}

are shown in Fig. 1a and 1d. Only the pattern of typical crystalline HAP (JPDS 00-09-0432) can be individuated without presence of lines typical of the most stable iron oxide/hydroxide phases. The introduction of iron species by *flash* ion exchange influenced the morphological properties of the samples, *i.e.*, surface area, pore volume and pore size distribution (Table 1). As a general trend, a slight increase in the specific surface area and pore volume values was observed after iron functionalization of HAP, whereas mean pore radius decreased. Moreover, the higher the loading, the more significant were the differences compared to bare HAP.

Although a different aggregation state of the iron species was expected when deposition-precipitation (DP) and wetness impregnation (WI) procedures were employed to functionalize HAP surface, XRPD analysis allowed to rule out the growth of Fe-aggregates and/or crystalline iron phase in these samples. Indeed the hydroxyapatite was the unique detectable crystalline phase in all the obtained diffractograms of the Fe-samples prepared by DP and WI (Fig. 1, b and c). On the other hand, more pronounced variations in the morphological features among the samples could be observed. Similarly to Fe/HAP_{IE} catalyst series, an increase in the specific surface area values associated with an increase in pore volume and a decrease of mean pore radius were detected also in this case.

To assess the complete removal of residual precursors, thermogravimetric analysis (TGA) was carried out on both the dried and calcined Fe/HAP samples. The TGA analyses (Fig. S2) in the temperature range from 35 to 500°C revealed only water desorption in an amount lower than 5 wt.% for the dried and lower than 2.5 wt.% for the calcined samples prepared by *flash* ionic exchange and deposition-precipitation. Conversely, the TGA analyses of the dried Fe/HAP_{WI} samples (Fig. S2, f and g) revealed also the additional presence of other mass loss events, likely due to nitrate species decomposition. Anyway, TGA results on the calcined samples confirmed the complete removal of nitrates after calcination.

The Fe/HAP samples are expected to possess well developed acidic sites thank to the dispersed iron phase on hydroxyapatite surface, which is an amphoteric surface with both basic and acid sites

[19]. Acidity measurements have been performed by adsorption of ammonia, chosen as basic probe for its high basicity (Proton Affinity 8.53 kJ·mol^{-1}) and because it is a reagent of our studied reaction. Table 1 reports the results obtained in terms of total amount of adsorbed ammonia. As expected, the acidity of HAP increases by iron addition, independently of the used method of iron deposition. In particular, a well increasing trend of acidity with the iron concentration has been observed for the samples prepared by ion exchange method (HAP/500 << Fe2/HAP$_{IE}$ < Fe5/HAP$_{IE}$ < Fe7/HAP$_{IE}$). Results do not follow the same trend of the iron amount in the samples, with no regular increase of acidity with iron concentration (Table 1). The first iron addition on HAP (Fe2/HAP$_{IE}$) led to a very high increase of the acid sites, while a lower increase of acidity was observed for the successive Fe-additions (Fe5/HAP$_{IE}$ and Fe7/HAP$_{IE}$). Likely, the first amount of added Fe^{3+} could be accomodated on the HAP surface and/or in the exchange Ca(I) or/and Ca(II) positions of HAP, then, some degree of aggregation of the Fe phase could occur for further Fe-addition. For the samples prepared by deposition-precipitation and wetness impregnation methods, a more limited acidity has been determined (HAP/500 < Fe5/HAP$_{DP}$ ≤ Fe7/HAP$_{DP}$ and (HAP/500 < Fe5/HAP$_{WI}$ < Fe7/HAP$_{WI}$). For these samples, it can be guessed some more aggregation of the iron centers on the HAP surface than on the samples prepared by ion exchange.

NH_3-SCR catalytic results

The intrinsic amphotericity of HAP support together with the redox activity of iron centres makes Fe/HAP samples promising candidates as NH_3-SCR catalysts, as already presented in a recent paper [13]. HAP possesses both acid sites (attributed to Ca^{2+}, surface HPO_4^{2-} and OH^- vacancies) and basic sites (associated with PO_4^{3-}, OH^-) which can interact with NH_3 and NO, respectively, thus contributing to increase their surface concentration, which could give positive consequence on catalytic activity.

It is also known that the procedure for metal addition on hydroxyapatite surface can affect the catalytic behaviour of the obtained samples, as reported for Cu/HAP [11]. Herein, the catalytic

performances of Fe/HAP samples prepared by the three different procedures have been evaluated in the NH_3-SCR reaction in the 120-500°C interval, working at fixed contact time (0.12 s) and starting, at first, from an equimolar NH_3/NO mixture.

Profiles of conversion of the fed species (NO_x and NH_3) and selectivity to the main products obtained on all the Fe/HAP samples are reported in Fig. 2 and Fig. 3 as a function of the reaction temperature. All the catalysts were active in the NH_3-SCR reaction. In particular it can be observed that a low Fe-concentration on HAP was sufficient to impart good de-NO_x activity to HAP. Actually, when tested as catalyst, bare HAP gave only *ca*. 20% of NO_x conversion in the range 300-400°C (Fig. S3) thanks to the above described acidic and basic sites of HAP, while the addition of only 2 wt.% of iron gave a sensitive increase of conversion up to approximatively 55% (Table 2). On the other hand, increasing the Fe-concentration from 2 wt.% up to 7 wt.% did not lead to clear differences in the catalyst conversion/selectivity and in general the optimal iron concentration seems to be *ca*. 5 wt.% (Table 2).

Concerning the formed products from NO_x conversion, in all the cases N_2O was the only observed species besides N_2. It has to be remarked that in general a very high selectivity to dinitrogen has been obtained even in the presence of strong oxidizing conditions (10,000 ppm of O_2). However, some interesting differences emerged when catalysts prepared by different procedures were compared. For the samples prepared by *flash* ionic exchange (Fig. 2, a-c), the maximum NO_x conversion was attained between 300 and 400°C (Table 2); above this temperature the unselective NH_3 oxidation occurred with undesired formation of N_2O. Consequently, the selectivity to N_2 was very high (98%, Table 2) up to 400°C, while it gradually decreased down to 85% in the range 400-500°C due to non negligible formation of N_2O (*ca*. 15% of selectivity to N_2O at 500°C, Table 2). Differently, the samples prepared either by deposition-precipitation or by wetness impregnation (Fig. 3) reached a maximum NO_x conversion at lower temperature (*ca*. 300-350°C, Table 2), compared to the Fe/HAP_{IE} samples. At higher reaction temperatures (T > 350°C), NH_3 started to be oxidised to N_2O with a deep drop of NO_x conversion to N_2. Hence, a higher selectivity to N_2O was observed (*ca.* 25-35% at 500°C, Table 2) to

the detriment of N_2 selectivity, which decreased down to 70% at 500°C. Therefore, from the comparison among the three catalyst series, it emerges that Fe/HAP_{IE} were more able to selectively convert NO_x to N_2 in a broader temperature window than Fe/HAP_{DP} and Fe/HAP_{WI}. The peculiar behaviour of Fe/HAP_{IE} catalysts could be ascribed to the speciation of the iron phase, dispersed Fe^{3+} centers being the principal species on all the Fe/HAP_{IE} surfaces (see *next paragraph*).

The effect of feeding NH_3/NO ratio on NO_x conversion has also been investigated by exploring the catalytic performances of Fe/HAP catalysts in the presence of an excess or a defect of ammonia (Table 2). As expected, a defect of NH_3 in the fed gases (NH_3/NO=0.6) led to a moderate conversion of NO_x associated with high NH_3 conversion, if evaluated at temperature of maximum NO_x conversion, independently of Fe-loading, as observed on Fe/HAP_{IE} samples. On the opposite, any clear positive effect on NO_x conversion or N_2 selectivity cannot be observed working with an excess of NH_3 in the fed gases (NH_3/NO=2) on all the catalysts. A closer look to the results obtained working with NH_3/NO=2 showed that on the highest Fe-concentrated catalysts (Fe7/HAP_{DP} and Fe7/HAP_{WI}) an increase of NO_x conversion occurred (Fig. 4, d and f; and Table 2). Also in this case, an effect of iron speciation could be guessed to justify this behaviour (see *next paragraph*).

An insight on the role of Fe-concentration on the catalytic performances has been attempted by computing specific activity, expressed as $mol_{N2}\cdot(mol_{Fe}\cdot s)^{-1}$ (Table 2, column 7). A decreasing trend in calculated values emerged as a function of iron concentration for all the Fe/HAP samples, in particular for the Fe/HAP_{IE} catalysts. This could be related to the different sitting and accessibility of Fe species. Indeed, it is reasonable to assume that increasing the amount of iron introduced on HAP, iron centers should be located not exclusively at the surface, but also in the bulk positions of HAP, thus reducing their exposure and accessibility. Catalyst acidity evaluation also strenghtened this consideration, as higher number of acid sites was not determined on the iron catalysts at higher Fe-concentration (see *next paragraph*). Moreover, comparing the samples at similar Fe-loading, higher values of specific activity have been observed on samples prepared by deposition-precipitation and wetness impregnation. It can be deduced that a judicious degree of metal aggregation is beneficial for

the NO_x conversion. In any case, increasing the iron loading did not have positive consequences on de-NO_x activity. Actually, an increase in iron concentration does not imply a higher exposure of active sites.

A full understanding of these catalytic results cannot prescind from a detailed characterisation in terms of iron nucleation and speciation. For this reason, a combination of Mössbauer and UV-DRS spectroscopies was used to investigate the nature, structure and aggregation of the iron species of the Fe/HAP catalysts.

Studies on Fe speciation in relation with catalytic activity of Fe/HAP

The Mössbauer spectra of the Fe/HAP_{IE} samples collected at room temperature (25°C) and their hyperfine parameters are reported in Fig.S4 (a-c) and Table S2, respectively. All the spectra presented only two peaks in the central region, so the fitting was realised using two doublets. In any case, low values of the isomer shifts (δ) were detected, typical of Fe^{3+} species. The doublets of all the three Fe/HAP_{IE} samples with lower isomer shifts (Table S2), which correspond to red lines in Fig. S4 (a-c), have quadrupole splittings (Δ) significantly higher than the other doublets, corresponding to blue lines in Fig. S4 (a-c). Both doublets could be produced by: *(i)* very small iron oxides crystallites with superparamagnetic behavior, the doublet with higher Δ value could be assigned to iron ions located in the shell of the nanoparticles (with a surrounding highly asymmetric) and the other to iron ions located inside the core of the nanoparticles; or *(ii)* paramagnetic Fe^{3+} ions exchanged with Ca^{2+} ions and/or complexed by surface phosphate/carbonate groups. In this case, the iron ions exchanged would produce two doublets with different Δ values due to the nonequivalent sites of Ca^{2+} (Ca(1) and Ca(2)), exchangeable and with different symmetries, present on the HAP lattice.

With the aim to discern between both alternatives, Mössbauer spectra of Fe/HAP_{IE} samples were collected at -260.15°C (13 K) (Fig. 5, a-c). Also in this case, all the spectra presented a central signal with two peaks. However, at -260.15 °C the superparamagnetic relaxation of iron oxides nanoparticles should be totally or partially blocked, thus a sextuplet or a curved background must be

present in the spectra. Consequently, it can be deduced that all catalysts prepared by *flash* ionic exchange procedure, independently of the Fe-loading, have high concentration of paramagnetic Fe^{3+} ions that replaced to the Ca^{2+} ions and/or complexed by surface phosphate/carbonate groups. As already done for the spectra at room temperature, the fitting was realized using two doublets. Jiang et al. [20] presented a theoretical and experimental study of the HAP exchanged with Fe^{2+} and Fe^{3+} ions and they demonstrated that the Fe^{3+} ions can replace both Ca(2) and Ca(1) ions. Bearing in mind the HAP structure [8], the surrounding of the sites Ca(2) is more symmetric than that corresponding to Ca(1). This different geometry would explain the difference between Δ values of the two doublets (Table 3). This hyperfine parameter reflects the symmetry of the site where the iron atoms are located. A greater asymmetry produces a higher electric field gradient and, as a consequence, a greater Δ value.

The quantitative evaluation of the population of both sites was realized at -260.15°C (13 K) (Table 3) because the areas of both calculated doublets at 25°C have important errors, due to the high overlapping of the two doublets. Then, considering that the difference between the recoil free fractions of both sites are negligible at very low temperatures, it can be concluded that the Ca(1) site is preferentially occupied by Fe^{3+} ions (ratio of about 1.5), according to Ref. [20] and this ratio did not change when the iron loading is increased from 2 to 7 wt.%. These interesting results confirm the high exchange capability of the HAP: it is possible to functionalize it up to 7 wt.% of iron without having iron oxide nanoparticles, this in agreement with what reported in Refs. [21-22].

With the aim to check the absence of iron oxides compounds by an independent technique, a measure of magnetization (M vs. H) at room temperature of $Fe7/HAP_{IE}$ was performed (Fig. S5). A straight line was obtained up to external magnetic field of 20 kOe. This magnetic behavior is characteristic of paramagnetic materials. This result reinforces the conclusion that the only iron species are present as isolated Fe^{3+} ions. From fitting the experimental points, the slope of the straight

line leads to a magnetic susceptibility value (χ_g) of 1.05 x 10^{-4} emu·(g·Oe)$^{-1}$. The same conclusion could be obtained with the other samples which have lower iron loadings.

Concerning the samples prepared by deposition-precipitation and wetness impregnation, different results were obtained. On two samples prepared by impregnation, it was observed that both Mössbauer spectra and the hyperfine parameters collected at room temperature (Fig.S4, f-g, and Table S2, respectively) are very similar to those of Fe/HAP$_{IE}$ samples, while the situation was different for the spectra collected at -260.15°C (13 K) (Fig. 5, f-g). In order to facilitate the discussion, the Fe7/HAP$_{WI}$ sample will first be analyzed. The spectrum of this sample showed a pronounced broadening of the central signal with a curved background, typical of the presence of species with a partial magnetic blocking. For this reason, the fitting process was approached with a relaxing sextuplet and two doublets (green and blue and red lines, respectively). It must be emphasized that, if the iron ions are in extremely small oxide particles, the resulting magnetic moment does not remain fixed in the space. Instead of this, it can be "jumping" between two easy magnetic directions. The frequency of this "jumping" depends on the size of the nanoparticles, the temperature of the measurement, the iron oxide species, etc. Therefore, the sextuplet can collapse, following different line shapes which will depend on the frequency of the "jumping" of the magnetic moment. In the present samples the relaxing sextuplet has collapsed to a broad central singlet (Fig. 5, f and g, green interaction). Previous reports of the literature [23] indicate that amorphous iron oxide nanoclusters of about 4 nm size produce, at -268.15°C (5 K), hyperfine parameters very similar to those found for the sextuplet (green line in Fig. 5 g). The hyperfine parameters do not depend strongly on the temperature, when sufficiently low temperatures were reached. Therefore, the obtained parameters at -260.15°C (13 K) can be compared with that given by Bødker et al. [23] at -268.15°C (5 K) and it can be concluded that a fraction of iron species in Fe7/HAP$_{WI}$ would be present as amorphous iron oxide. However, if the features of the spectrum showed by these authors are compared with the spectrum of Fe7/HAP$_{WI}$ at -260.15°C (13 K), it can be seen that their clusters, of about 4 nm, are almost completely magnetically blocked. On the opposite, in Fe7/HAP$_{WI}$ a very wide central signal and a

curved background (green line in Fig. 5 g) only appear. This results would indicate the presence of nanoclusters with size lower than 4 nm because the magnetic blocking process is beginning at this point. Moreover, amorphous iron oxide nanoclusters of about 2 nm show, fundamentally, a superparamagnetic behavior at -268.15°C (5 K) and a temperature as low as -273.07°C (0.08 K) is necessary to get the complete magnetic blocking [24]. Therefore, it could be concluded that about 70% of the iron loading in Fe7/HAP_{WI} is present as amorphous iron oxides nanoclusters larger than 2 nm and smaller than 4 nm, because they have a higher magnetic blocking degree in comparison with what reported by Bauminger et al. [24]. The remaining iron loading is exchanged and/or coordinated in the same way that in the samples prepared by *flash* ionic exchange (red and blue interactions of Fig. 5 a-c). For Fe5/HAP_{WI} the same fitting procedure was followed but, the percentage of amorphous iron oxides nanoclusters is significantly decreased with respect to Fe7/HAP_{WI} (30 ± 3 % *vs*. 73 ± 3 %, for Fe5/HAP_{WI} and Fe7/HAP_{WI}, respectively, Table 3). Therefore, the wetness impregnation procedure does not allow reaching exchanged iron levels as high as that obtained by the *flash* ionic exchange method. Thus, when the HAP is loaded with 5 % of iron, the clustering is already detected.

The Mössbauer spectra collected at room temperature of the two Fe/HAP_{DP} samples showed only a central doublet (Fig. S4, d-e). On the other hand, the spectra collected at -260.15°C (13 K) were completely different: they clearly presented six peaks with an additional central peak and a background slightly curved (Fig. 5, d-e). This could be related to the presence of iron oxides species with different magnetically blocking degrees. Therefore, the fitting was performed with three sextuplets: two of them almost completely magnetically blocked and the remaining just partially blocked. The hyperfine parameters of the sextuplet with the higher magnetic field (associated with red lines in Fig. 5) are typical of α-Fe_2O_3 without Morin transition ($2\varepsilon \cong 0$ mm·s^{-1}) [25-26]. This is a magnetic transition that happens at -8.15°C (265 K) when bulk hematite changes from an antiferromagnetic state (below -8.15°C (265 K)) to a weakly ferromagnetic state (above -8.15°C (265

K)) but it does not occur in nanoparticles of α-Fe_2O_3 which size is lower than 20 nm. Therefore, it is possible to determine that in both catalysts this species has a size lower than 20 nm [27]. Another effect widely reported in literature for very small magnetic crystals of diverse iron oxides is the decreasing of the hyperfine magnetic field with respect to the corresponding bulk values present. Mørup and Topsøe developped a model named *collective magnetic excitations*, which allows to explain decreasing of magnetic hyperfine fields from 5 to 15% with respect to bulk compounds [28]. Using this model [29] and a value of anisotropic magnetic basal constant of 2.37 x 10^4 $J \cdot m^{-3}$, characteristic of hematite nanoparticles of about 6 nm [30], a rough size of the α-Fe_2O_3 nanoparticles present in Fe/HAP_{DP} catalysts can be obtained; the value calculated in this way is *ca.* 4.5 nm. This size is consistent with the fact that this species was not detected by XRPD. The second sextuplet (associated with blue lines in Fig. 5) can be assigned to nanoclusters of amorphous Fe_2O_3 by comparison with the results described by Bødker et al. [31] and using similar arguments than for $Fe7/HAP_{WI}$. The features of the second sextuplet for $Fe5/HAP_{DP}$ and $Fe7/HAP_{DP}$ are very similar to that reported by these authors for iron oxide nanoclusters of about 4 nm. Therefore, this iron oxide fraction should have a higher size than that represented by the relaxing sextuplets (green lines in Fig. 5 f-g) in $Fe5/HAP_{WI}$ and $Fe7/HAP_{WI}$. This conclusion is coherent with a higher magnetic blocking degree showed by the iron nanoclusters in $Fe5/HAP_{DP}$ and $Fe7/HAP_{DP}$. The third sextuplet (associated with green line in Fig. 5 d-e) of the two Fe/HAP_{DP} samples show a very similar shape to that present in $Fe5/HAP_{WI}$ and $Fe7/HAP_{WI}$ at -260.15°C (13 K). Therefore, following the same arguments, this sextuplet can be attributed to amorphous iron oxide nanoclusters lower than 4 nm and higher than 2 nm.

Finally, all the prepared Fe/HAP samples have been analyzed by UV-Vis-DR spectroscopy to confirm the results suggested by Mössbauer spectroscopy concerning iron speciation on HAP surface.

The UV-Vis DR spectra of all Fe/HAP samples were recorded at room temperature in the 200-1200 nm range; they are displayed in Fig. 6 limited to the 200-800 nm region. Different absorption bands typical of iron species were observed in this region and they can be ascribed to ligand to-metal

charge transfer (CT) excitations, from O (2*p*) nonbonding valence bands to Fe (3*d*) ligand field orbitals ($O^{2-} \rightarrow Fe^{3+}$), or to Fe^{3+} *d-d* (ligand field) transitions. All the spectra were characterised by an apparent complexity due to the overlapping of different signals; therefore, the decomposition in *sub*-bands has been pursued to identify the different contributions.

In general, all the spectra are dominated by two features: *i)* strong absorption in the 250-280 nm range, assigned to the CT transitions, due to the presence of isolated Fe^{3+} centres, and *ii)* broad absorption in the 460-550 nm range, corresponding to *d-d* transitions from ground state ($^6A_1$) to excited ligand field states ($^4T_1$ or $^4T_2$ or ^4E) (Table S3). In general, as the *d-d* transitions are spin forbidden, they are characterized by weak intensity, while more intense bands could be observed if iron clusters in some aggregate form are present, in which the magnetic coupling occurs between adjacent Fe^{3+} ions [32]. However, the attribution of these bands at high wavelength (> 400 nm) is debated in the literature where they have been attributed to *d-d* or CT transitions of Fe_xO_y oligomers on several iron exchanged zeolites [33, 34].

Moreover, another band at *ca*. 200 nm was observed in all the Fe/HAP spectra that could be assigned to $O^{2-} \rightarrow Ca^{2+}$ charge transfer excitations, typical of Ca^{2+} sites located on the HAP surface; this band is particularly visible in the spectra of the Fe/HAP_{WI} series samples and on bare HAP (Fig. S6).

Interestingly, the UV-Vis-DR spectra of all Fe/HAP_{DP} and Fe/HAP_{WI} possessed more intense *d-d* transition bands than the spectra of the Fe/HAP_{IE} samples. This evidence confirms the high dispersion of the Fe-phase, predominantly present as isolated Fe^{3+} centres with very limited aggregation, of the Fe/HAP_{IE} samples, and the presence of some Fe_xO_y aggregates of the Fe/HAP_{DP} and Fe/HAP_{WI} samples, as observed from Mössbauer spectroscopy. The detailed spectroscopic attributions for the samples are reported in Table S4.

The evaluation of the reducibility of different iron species present in the materials represents a powerful tool helping to establish meaningful relations between the variegated iron speciation in the Fe/HAP samples and the corresponding catalytic behaviour in the NH_3-SCR reaction, which is

governed by electron exchanges. Temperature programmed reduction experiments (H_2-TPR) have been carried out to investigate the reduction behaviour of the Fe-phase of the Fe/HAP samples. TPR profiles and characteristic features (maximum temperatures of hydrogen consumption and H_2/Fe molar ratios) are reported in Fig.S5 and Table 4, respectively. It is known that the reduction of iron species can occur according to different pathways including several intermediate steps. In addition the reducibility of iron centers strongly depends on the crystallite size and on the interactions with the support. This intrinsic complexity makes difficult any tentative attribution of TPR signals of our samples. Nevertheless, the information deriving from Mössbauer and UV-DR spectroscopies together with the literature results can help in interpreting the obtained profiles. In particular, the samples prepared by ion exchange procedures exhibit small peaks in the region between 470 and 550°C, corresponding to a very low H_2 consumption. These signals could be ascribed to the reduction of isolated Fe^{3+} centers to Fe^{2+}. It is noteworthy that the same signals are individuated in the samples prepared by incipient wetness, even if additional reduction peaks are present in these catalysts at higher temperature. These results confirm the spectroscopic evidences, which suggest that incipient wetness method can lead in part to isolated centers and in part to iron oxide aggregates. Differently, these reduction peaks are not present in the samples prepared by deposition precipitation procedure. In this case, the presence of reduction peaks below 450°C (at ca. 375 and 400°C) may be consistent with the presence of large Fe_2O_3 aggregates, which are easily reduced to Fe_3O_4 and then to stable FeO species. These TPR signals below 450°C are also present in the samples prepared by wetness impregnation, thus supporting again the speciation from Mössbauer results, which indicates the presence of Fe_2O_3 aggregates in these samples.

The sample prepared by deposition-precipitation possessed the most reducible species (likely large Fe_2O_3 aggregates), in terms of hydrogen consumption (H_2/Fe molar ratio of *ca*. 1.2-1.4). On the contrary, ion exchange procedure produced iron samples characterized by a low reducibility (H_2/Fe molar ratio of *ca*. 0.2).

4. Conclusions

In this work, three different preparative methods (*flash* ionic exchange, deposition-precipitation and wetness impregnation) have been investigated for the preparation of Fe/HAP samples along with the effect of iron loading and both influenced the final aggregation states and the nature of iron species.

The catalytic behavior resulted to be affected by the iron accessibility onto HAP surface. In particular, a very low amount of Fe on HAP (ca. 2 wt.%) is sufficient to impart de-NO_x activity to HAP, whereas further Fe-addition (5-7 wt.%) does not induce a proportional improvement on the catalytic performances. Likely, a reduced accessibility of iron centers, which are not exclusively located at the HAP surface is responsible of the modest contribution of high Fe-loading.

Actually, the predominant presence of Fe^{3+} highly dispersed on HAP surface on samples prepared by ionic exchange assured a high selectivity to N_2 and a satisfactory activity in a large temperature interval. The prevalence of iron aggregates on HAP caused a not negligible formation of N_2O as main product of the unselective ammonia oxidation occurring at temperature higher than 350°C.

In conclusion, the optimization of iron dispersion on the HAP surface seems to be a suitable route to follow for the achievement of active and selective Fe/HAP catalysts for the NH_3-SCR process. Further investigations will be devoted to the study of these materials under real conditions (presence of water and sulfur).

Acknowledgements

Solvay, Soda Ash and Derivatives, Rue de Ransbeek 310, Bruxelles, is gratefully acknowledged for supplying hydroxyapatite, in particular Dr. Thierry Delphanche, Capterall® Technology Manager.

Dr. S. Campisi is grateful to MOPGA Program, edition 2018, which supported his stage at IRCELYON-CNRS (France).

The use of instrumentation purchased through the SmartMatLab Project of Dipartimento di Chimica (Cariplo Foundation, project 2013-1776) is gratefully acknowledged and also Dr. Daniele Marinotto of Consiglio Nazionale delle Ricerche (CNR), Istituto di Scienze e Tecnologie Molecolari (ISTM). Mrs. Iolanda Biraghi is acknowledged for her experimental support.

Conflicts of interest

There are no conflicts to declare.

References

[1] W. Wardencki, J. Curylo, J. Namiesnik, *Polish Journal of Environmental Studies* **2005**, *14*, 389-395.

[2] R.J. Farrauto, R.M. Heck, *Catal. Today* **1999**, *51*, 351-360.

[3] P. Forzatti, *Appl. Catal. A Gen*. **2001**, *222*, 221-236.

[4] T. Delplanche, A. Gervasini, US provisional patent application 62/431406 (2016) and PCT application publication WO2018/104445 (2018).

[5] T. Delplanche, A. Gervasini, US provisional patent application 62/431407 (2016) and PCT application publication WO2018/104446 (2018).

[6] T. Delplanche, A. Gervasini, US provisional patent application 62/543099 (2017) and PCT application EP2018/071493 (2018).

[7] H. Tounsi, S. Djemala, C. Petitto, G. Delahay, *Appl. Catal. B Environ.* **2011**, *107*, 158-163.

[8] A. Fihri, C. Len, R. S. Varma, A. Solhy, *Coordination Chemistry Review* **2017**, *347*, 48-76.

[9] T.J. Webster, E.A. Massa-Schlueter, J.L. Smith, B.E. Slamovich, *Biomaterials* **2004**, *25*, 2111-2121.

[10] B. Aellach, A. Ezzamarty, J. Leglise, C. Lamonier, J.-F. Lamonier, *Catal. Lett.* **2010**, *135*, 197-206.

[11] M. Schiavoni, S. Campisi, P. Carniti, A. Gervasini, T. Delplanche, *Appl. Catal. A Gen.* **2018**, *563*, 43-53.

[12] S. Diallo-Garcia, D. Laurencin, J.-M. Krafft, S. Casale, M. E. Smith, H. Lauron-Pernot, G. Costentin, *J. Phys. Chem. C* **2011**, *115*, 24317-24327.

[13] S. Campisi, M.G. Galloni, F. Bossola, A. Gervasini, *Catal. Comm.* **2019***, 123* () 79-85.

[14] P. Perrin, O.J.F.J.G. Bodson, T. Delplanche, D. Breugelmans, US Patent 0080401 (2017).

[15] M. Ferri, S. Campisi, M. Scavini, C. Evangelisti, P. Carniti, A. Gervasini, *Appl. Surf. Sci.* **2019**, *475*, 397-409.

[16] D.A.M. Monti, A. Baiker, *J. Catal.* **1983***, 83*, 323.

[17] A. Gervasini, in *Calorimetry and Thermal Methods in Catalysis* (Ed. A. Auroux), Springer, Berlin, **2013**, pp.175-195.

[18] K. Lagarec, D.G. Rancourt, Mössbauer *Spectral Analysis Software, Version 1*, Dep. of Phys-University of Ottawa, **1998**.

[19] L. Silvester, J.F. Lamonier, R. Vannier, C. Lamonier, M. Capron, A.S. Mamede, F. Pourpoint, A. Gervasini, F.Dumeignil, *J. Mater. Chem. A* **2014**, *2*, 11073-11524.

[20] M. Jiang, J. Terra, A.M. Rossi, M.A. Morales, E.M. Baggio Saitovitch, D.E. Ellis, *Phys. Review B* **2002**, *66*, 224107.

[21] E.R. Kramer, A.M. Morey, M. Staruch, S.L. Suib, M. Jain, J.I. Budnick, M. Wei, Synthesis and characterization of iron-substituted hydroxyapatite via a simple ion-exchange procedure, *J. Mater. Sci.* **2013***, 48*, 665–673.

[22] Y. Li, C.T. Nam, C.P. Ooi, *J. Phys.* **2009**, *187*, 12024.

[23] F. Bødker, S. Mørup, S. Linderoth, *Phys. Rev. Lett.* **1994**, *72*, 2.

[24] E. Bauminger, A. Levy, F. Labenski de Kanter, S. Ofer, C. Heintner-Wirg, Mössbauer spectra of iron containing nafion membranes, *J. Phys. Colloq.* **1980**, *41*, 329-330.

[25] E. Murad, J.H. Johnston, in *Mössbauer Spectroscopy Applied to Inorganic Chemistry Vol. 2* (Ed. G.J. Long), Plenum, New York, **1987**, pp. 507-582.

[26] L.H. Bowen, E. De Grave, R.E. Vandenberghe, in *Mössbauer Spectroscopy Applied to Magnetism and Materials Science Vol 1*, (Eds. G.J. Long and F. Grandjean), Springer, New York, **1993**, 115-160.

[27] R.E. Vandenberghe, E. De Grave, C. Landuydt, L.H. Bowen, *Hyperfine Interact*. **1990**, 53, 175–196.

[28] S. Mørup and H. Topsøe, , *Appl. Phys.* **1976**, *11*, 63-66.

[29] S. Mørup, *J. Magn. Magn. Mater*. **1983**, *37*, 39-50.

[30] F. Bødker, S. Mørup, *Europhys. Lett.* **2000***, 52*(2), 217-223.

[31] F. Bødker, S. Mørup, S. Linderoth, *Phys. Rev. Lett.* **1994***, 72*(2), 282.

[32] R.M. Cornell, U. Schwertmann, in *The Iron Oxides : Structure, Properties, Reactions, Occurrences and Uses*, Wiley-VCH, Weinheim, **2003**; pp 139–183.

[33] Kumar, M.S., Schwidder, M., Grünert, W., and Brückner, A. *J. Catal.***2004**, *227* (2), 384–397.

[34] Centi, G., Perathoner, S., Pino, F., Arrigo, R., Giordano, G., Katovic, A., and Pedulà, V. *Catal. Today* **2005**, *110* (3–4), 211–220.

10.1002/cctc.201901813

Table and Figures

Table 1

Main morphological and surface properties of Fe/HAP samples

Code	Fe Loading[b] (wt.%)	S.S.A.[c] ($m^2 \cdot g^{-1}$)	N[d]	Pore Volume[e] ($cm^3 \cdot g^{-1}$)	Mean Pore Radius[f] (nm)	Acidity[g] ($\mu moles_{NH3(ads)}\ g^{-1}$)
HAP/500[a]	-	53	2	0.19	8.2	126.6 ± 7
$Fe2/HAP_{IE}$	2.07	68	5	0.21	6.8	198.1
$Fe5/HAP_{IE}$	4.77	69	4	0.20	6.4	204.9 ± 2
$Fe7/HAP_{IE}$	6.83	76	85	0.24	6.4	218.0
$Fe5/HAP_{DP}$	4.26	84	11	0.24	6.7	145.2 ± 4
$Fe7/HAP_{DP}$	6.32	76	2	0.20	7.3	149.0
$Fe5/HAP_{WI}$	5.00	71	4	0.21	7.0	147.4 ± 9
$Fe7/HAP_{WI}$	7.00	64	4	0.19	6.6	151.3 ± 1

[a] bare HAP calcined at 500°C for 1 h; [b] obtained by atomic absorption; [c] Specific Surface Area determined by 3-parameters BET equation; [d] computed average number of adsorbed N_2 layers; [e] at $p/p^0=0.95$; [f] determined by BJH model from desorption branch of the isotherm ($0.3< p/p^0< 0.95$); [g] for repeated acidity tests, standard deviation is reported.

Table 2

Main catalytic results on Fe/HAP in NH_3-SCR reaction

Code	NH_3/NO	$T_{max.conv.NOx}$[a] (°C)	NO_x Conversion[b] (%)	NH_3 Conversion[c] (%)	N_2 Selectivity[d] (%)	10^4· Specific Activity[e] (mol_{N2}·(mol_{Fe}·s)$^{-1}$)
$Fe2/HAP_{IE}$	0.6	400	36.9	86.4	94.7	4.85
	1	350	49.8	51.9	97.6	6.32
	2	400	47.0	34.7	93.9	6.19
$Fe5/HAP_{IE}$	0.6	400	45.7	84.7	94.5	2.41
	1	400	65.1	73.2	95.4	3.54
	2	400	63.7	38.7	91.6	3.21
$Fe7/HAP_{IE}$	0.6	350	38.5	59.2	94.8	1.29
	1	400	56.6	64.1	94.1	1.86
	2	350	58.7	15.3	94.7	1.47
$Fe5/HAP_{DP}$	1	350	59.9	79.0	94.7	4.17
	2	350	51.6	41.5	92.9	3.31
$Fe7/HAP_{DP}$	1	325	61.1	81.7	95.1	2.63
	2	325	65.6	33.1	94.1	2.34
$Fe5/HAP_{WI}$	1	325	66.9	67.3	98.4	3.27
	2	350	66.4	31.0	96.0	2.75
$Fe7/HAP_{WI}$	1	350	48.9	70.2	96.6	1.97
	2	350	66.9	34.8	94.5	1.90

[a] temperature of maximum NO_x conversion; [b-e] evaluated at temperature of maximum NO_x conversion.

Table 3
Mössbauer parameters of Fe/HAP samples collected at -260.15 °C (13 K).

Code	Parameters					Fe species
	Δ^a (mm·s^{-1})	δ^b (mm·s^{-1})	$2\varepsilon^c$ (mm·s^{-1})	H^d (kOe)	%^{e}	
Fe2/HAP$_{IE}$	1.5 ± 0.1	0.55 ± 0.03	-	-	38 ± 6	Paramagnetic Fe^{3+} in Ca(2)/complexation
	0.73 ± 0.06	0.52 ± 0.02	-	-	62 ± 6	Paramagnetic Fe^{3+} in Ca(1)/complexation
Fe5/HAP$_{IE}$	1.4 ± 0.1	0.49 ± 0.02	-	-	35 ± 6	Paramagnetic Fe^{3+} in Ca(2) /complexation
	0.85 ± 0.04	0.52 ± 0.01	-	-	65 ± 6	Paramagnetic Fe^{3+} in Ca(1)/complexation
Fe7/HAP$_{IE}$	1.35 ± 0.07	0.51 ± 0.01	-	-	39 ± 6	Paramagnetic Fe^{3+} in Ca(2)/complexation
	0.82 ± 0.04	0.51 ± 0.01	-	-	61 ± 6	Paramagnetic Fe^{3+} in Ca(1)/complexation
Fe5/HAP$_{DP}$	-	0.50 ± 0.02	-0.05 ± 0.04	490 ± 2	60 ± 5	α-Fe_2O_3, *ca*. 4.5 nm
	-	0.43 ± 0.05	-0.1 ± 0.1	442 ± 6	32 ± 5	Fe_2O_3 nanoclusters, *ca*. 4 nm
	-	0.3 ± 0.1	0[f]	410[f]	8 ± 1	Fe_2O_3 nanoclusters, 4 < size (nm) < 2
Fe7/HAP$_{DP}$	-	0.47 ± 0.01	-0.01 ± 0.02	492 ± 2	75 ± 3	α-Fe_2O_3, *ca*. 4.5 nm
	-	0.45[f]	0[f]	451 ± 3	19 ± 3	Fe_2O_3 nanoclusters, *ca*. 4 nm
	-	0.4[f]	0[f]	410[f]	6 ± 1	Fe_2O_3 nanoclusters, 4 < size (nm) < 2

Fe5/HAP$_{WI}$	1.76 ± 0.05	0.49 ± 0.02	-	-	19 ± 3	Paramagnetic Fe^{3+} in Ca(2)/complexation
	1.02 ± 0.05	0.48 ± 0.01	-	-	51 ± 3	Paramagnetic Fe^{3+} in Ca(1)/complexation
	-	0.40 ± 0.02	0[f]	450[f]	30 ± 3	Fe_2O_3 nanoclusters, 4 < size (nm) < 2
Fe7/HAP$_{WI}$	1.63 ± 0.05	0.52 ± 0.02	-	-	13 ± 2	Paramagnetic Fe^{3+} in Ca(2)/complexation
	0.98 ± 0.06	0.49 ± 0.03	-	-	14 ± 2	Paramagnetic Fe^{3+} in Ca(1)/complexation
	-	0.39 ± 0.02	0[f]	450[f]	73 ± 3	Fe_2O_3 nanoclusters, 4 < size (nm) < 2

[a] quadrupole splitting; [b] isomer shift (all the isomer shifts are referred to α-Fe at 25 °C); [c] quadrupole shift; [d] hyperfine magnetic field; [e] normalized population of Fe^{3+} centers; [f] parameter held fixed in fitting.

10.1002/cctc.201901813

Table 4.

H_2-TPR results on Fe/HAP samples.

Code	Fe concentration ($mmol \cdot g_{Fe}^{-1}$)	T_{max}[a] (°C)	H_2 consumption ($mmol_{H2} \cdot g_{cat}^{-1}$)	H_2/Fe molar ratio
$Fe2/HAP_{IE}$	0.37	472 517	0.09	0.25
$Fe5/HAP_{IE}$	0.85	455 495 524 577 636	0.21	0.24
$Fe7/HAP_{IE}$	1.22	485 521 675	0.36	0.29
$Fe5/HAP_{DP}$	0.76	376 413 547 634 767	0.98	1.3
$Fe7/HAP_{DP}$	1.13	374 393 534 667 761 859	1.37	1.2
$Fe5/HAP_{WI}$	0.90	460 524 624 696 732 867	1.26	1.4
$Fe7/HAP_{WI}$	1.25	373 445 515 618 705 833	1.49	1.2

[a] temperature at peak maximum obtained from computation (Fig. S7).

10.1002/cctc.201901813

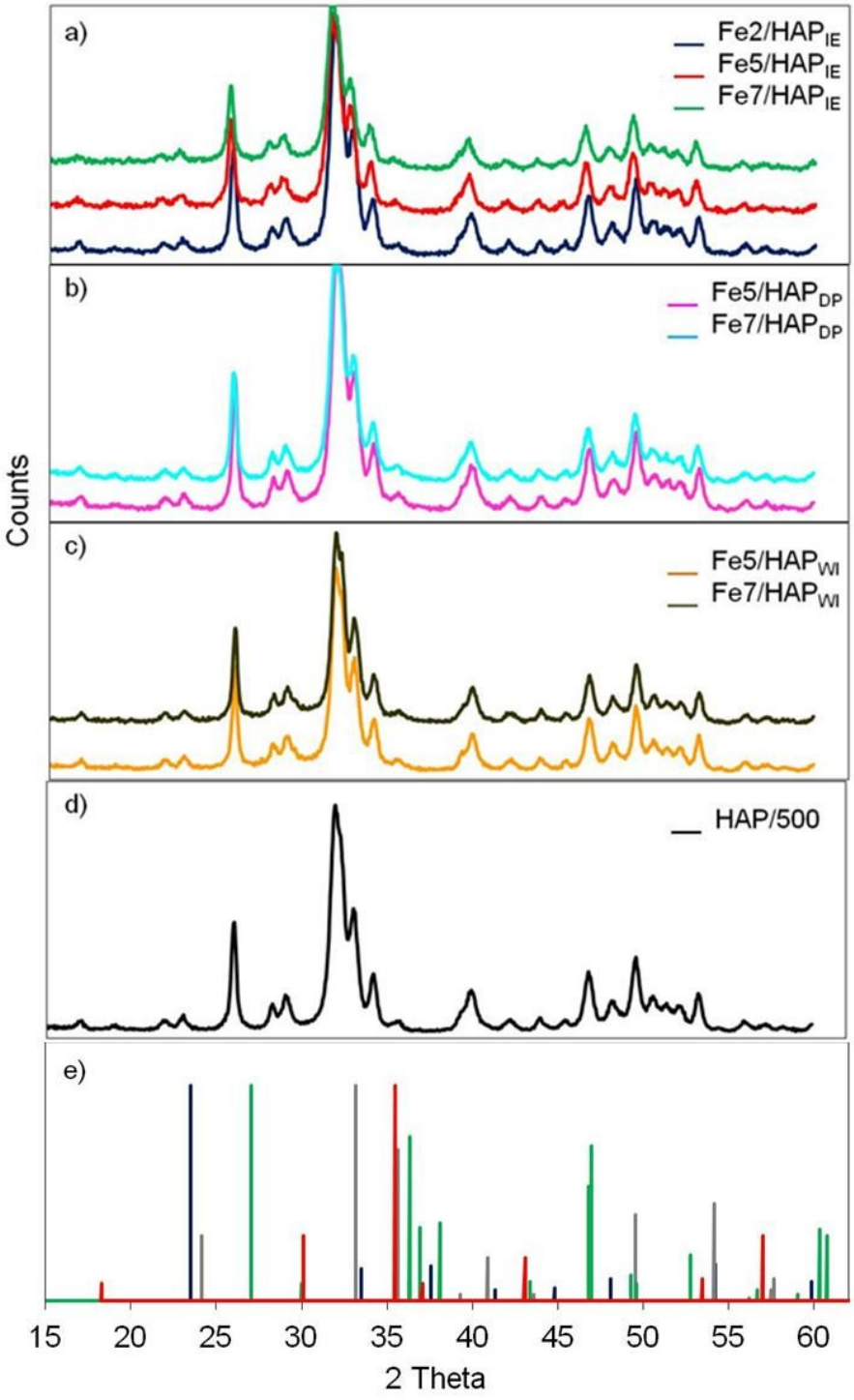

Fig. 1. XRPD patterns of Fe/HAP samples prepared by *flash* ionic exchange (a), deposition-precipitation (b), incipient wetness impregnation (c) and bare HAP (d) after calcination at 500°C. The diffraction patterns of iron oxide phases: $Fe(OH)_3$, bernalite, JCPDS 00-046-1436, blue; Fe_3O_4, magnetite, JCPDS 00-019-0629, red; ɣ-FeO(OH), lepidocrocite, JCPDS 00-044-1415, green; α-Fe_2O_3, hematite, JCPDS 00-033-0664, grey; are reported in panel (e) as reference

10.1002/cctc.201901813

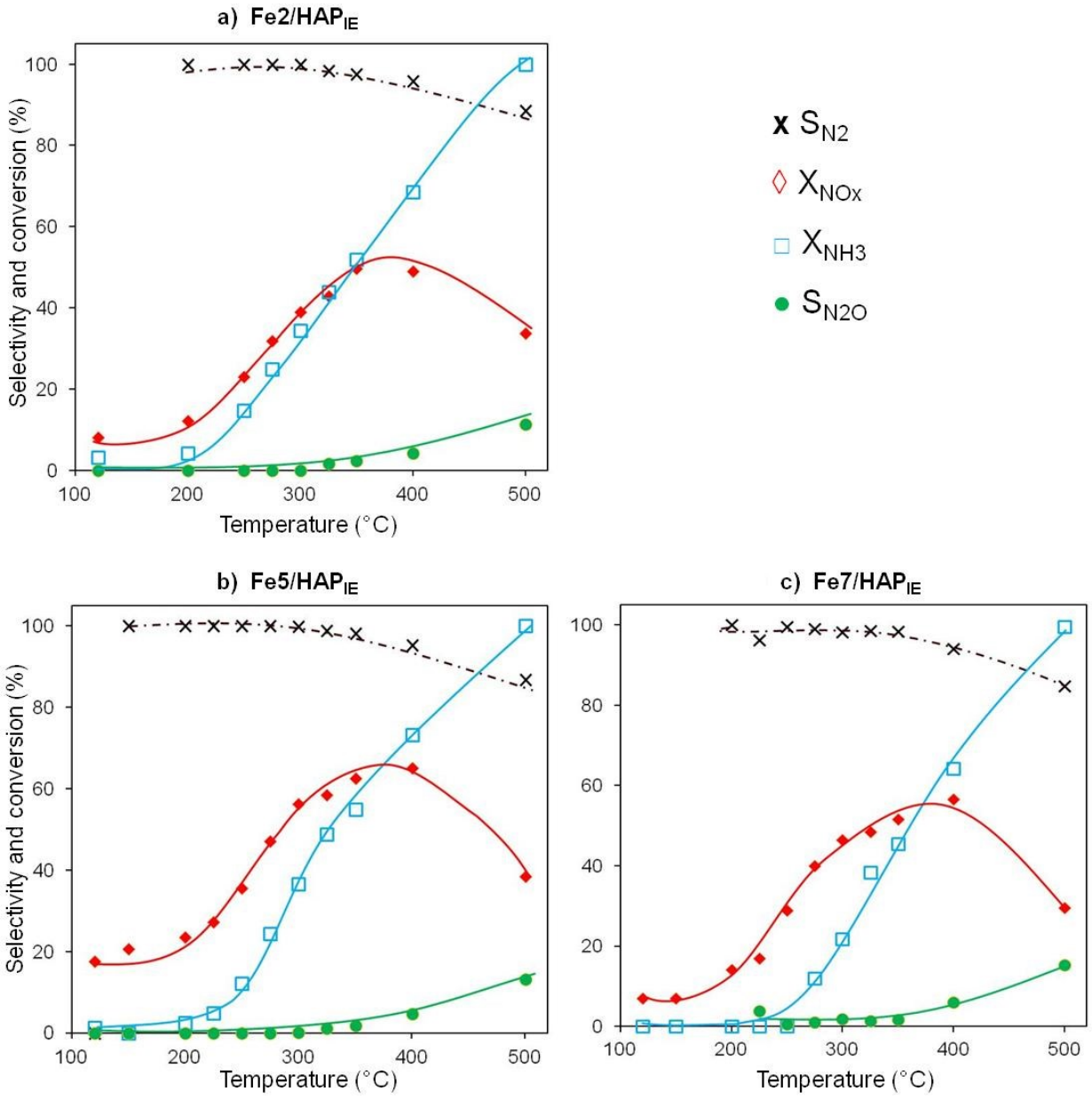

Fig. 2. NH_3-SCR catalytic results on Fe/HAP samples prepared by *flash* ionic exchange (a-c): profiles of conversion of the fed species (NO_x and NH_3) and selectivity of formed species (N_2 and N_2O) as a function of reaction temperature with the use of NH_3/NO ratio equal to one.

10.1002/cctc.201901813

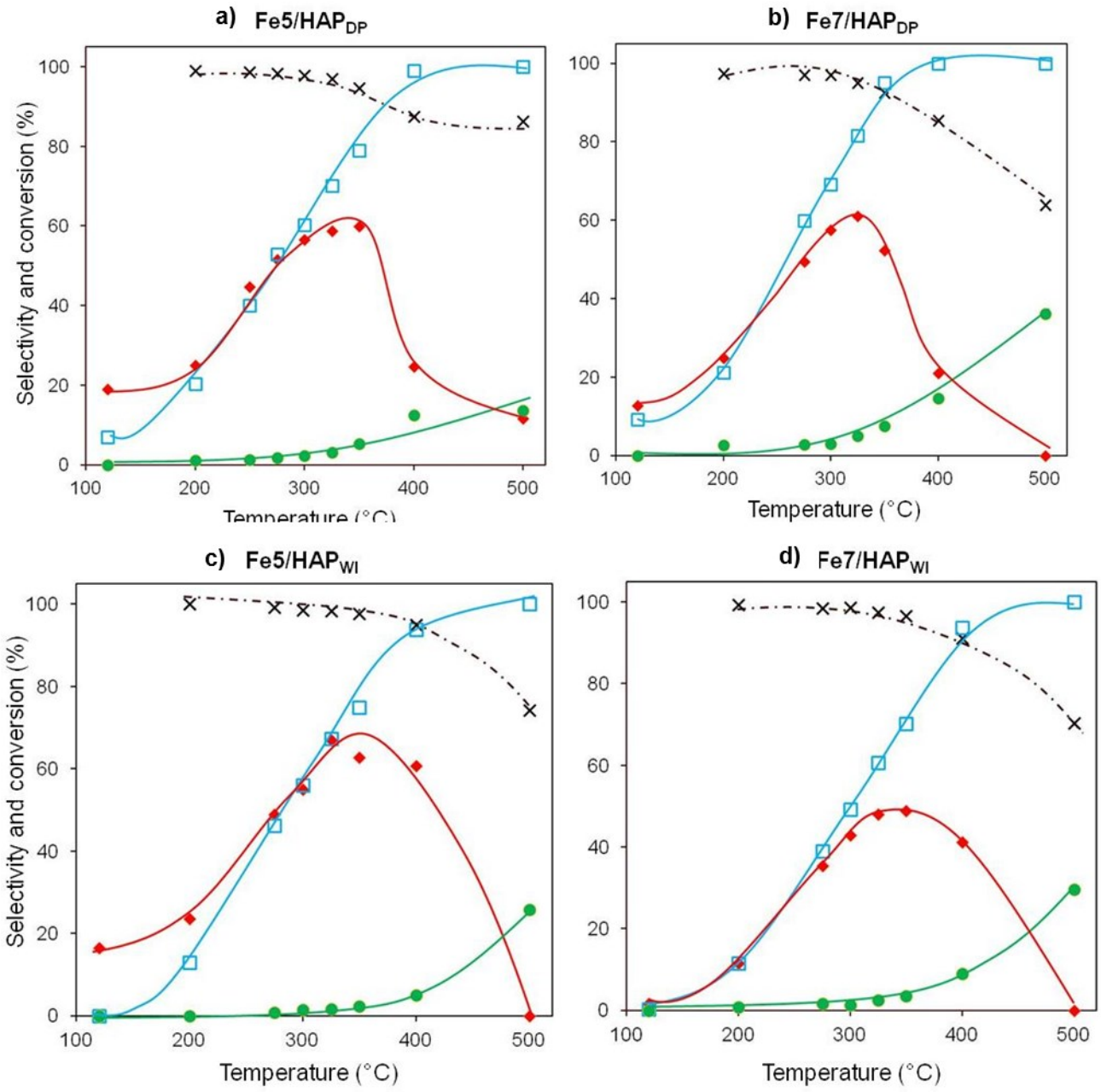

Fig. 3. NH_3-SCR catalytic results on Fe/HAP samples prepared by deposition-precipitation (a-b) and incipient wetness impregnation (c-d): profiles of conversion of the fed species (NO_x and NH_3) and selectivity of formed species (N_2 and N_2O) as a function of reaction temperature with the use of NH_3/NO ratio equal to one.

10.1002/cctc.201901813

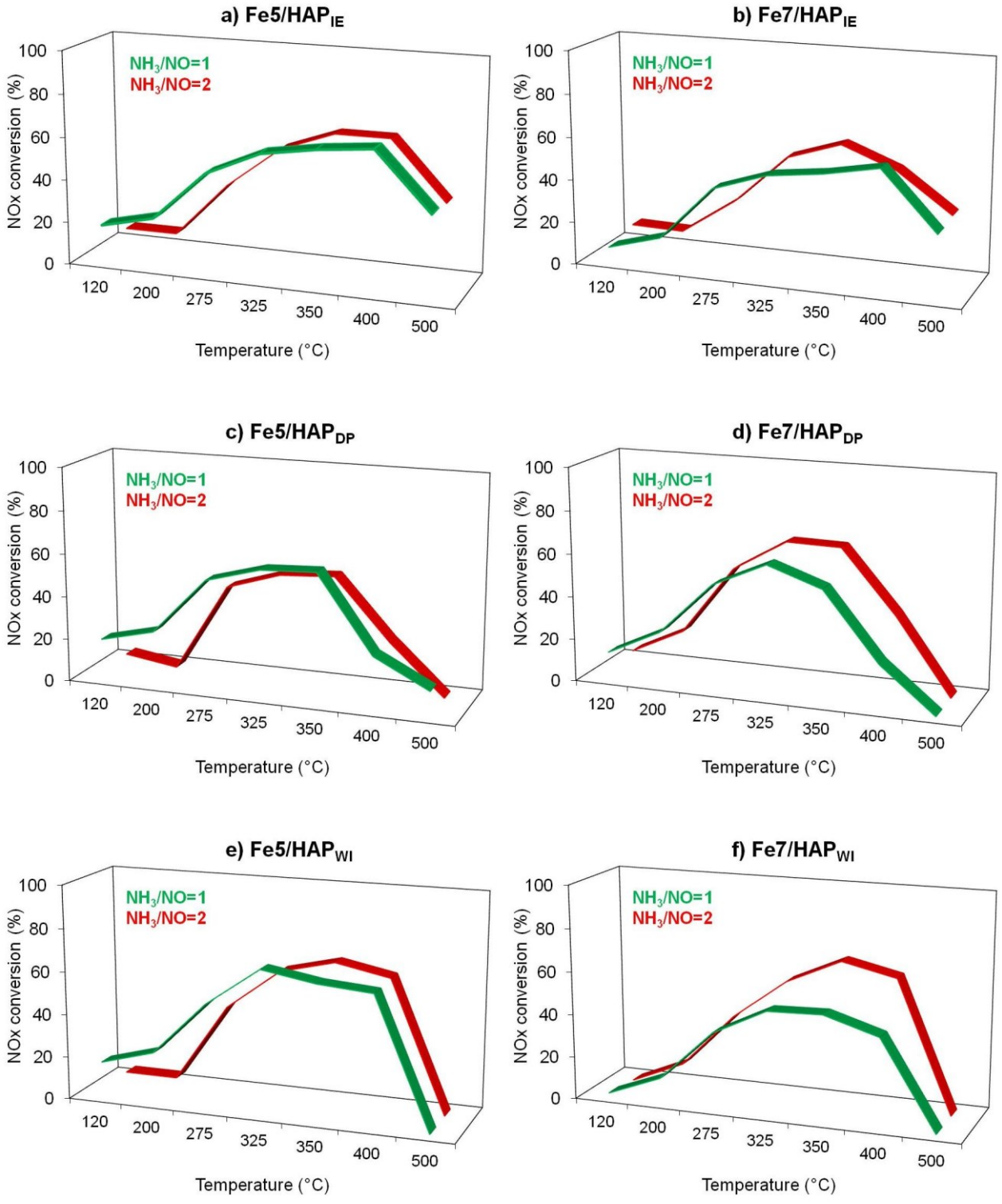

Fig. 4. NH_3-SCR catalytic results on Fe/HAP samples prepared by *flash* ionic exchange (a-b), deposition-precipitation (c-d) and incipient wetness impregnation (e-f): comparison of NO_x conversion as a function of reaction temperature at different ammonia concentrations (NH_3/NO=1, green and NH_3/NO=2, red).

10.1002/cctc.201901813

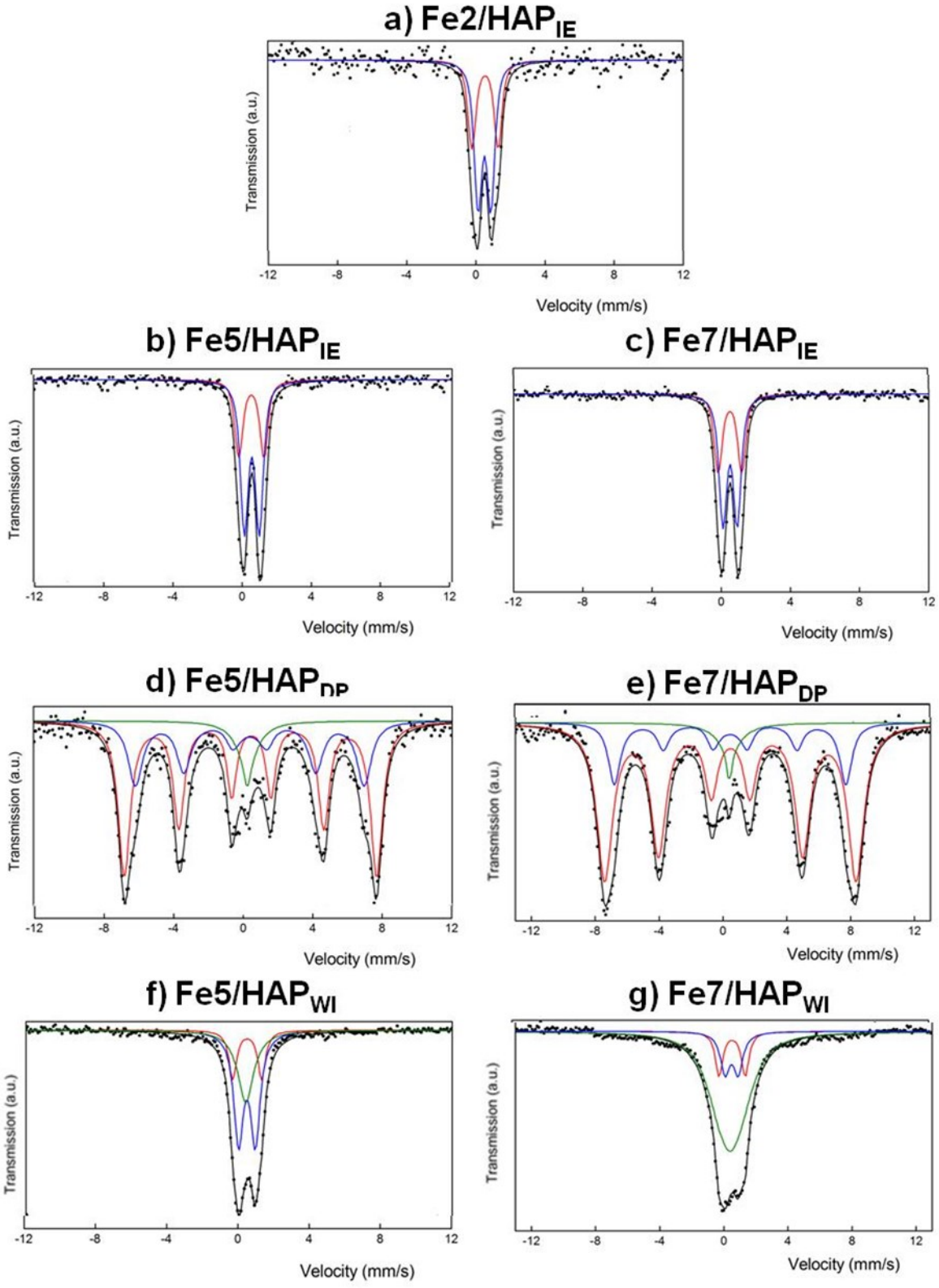

Fig. 5. Mössbauer spectra of Fe/HAP samples prepared by *flash* ionic exchange (a-c), deposition-precipitation (d-e) and incipient wetness impregnation (f-g) at -260.15°C (13 K). Black points are the experimental values; green, red, and blue lines are interactions obtained from fitting and assigned; and black lines are the convolution of all the interactions.

10.1002/cctc.201901813

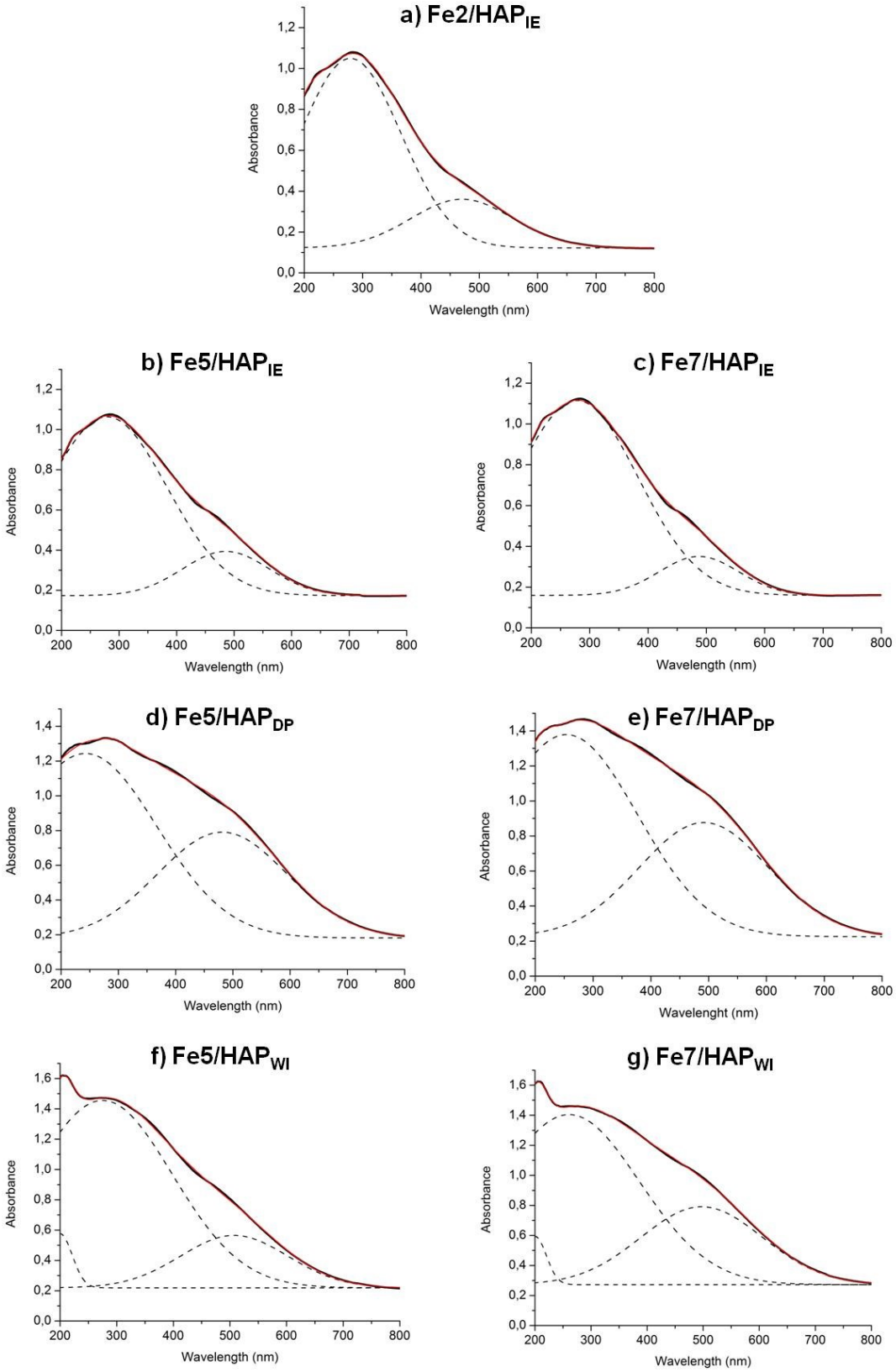

Fig. 6. UV-Vis-DR spectra (black curves) of Fe/HAP samples prepared by *flash* ionic exchange (a-c), deposition-precipitation (d-e) and incipient wetness impregnation (f-g). Total calculated curves (red lines) and decomposed curves (dotted black lines) are also reported..

10.1002/cctc.201901813

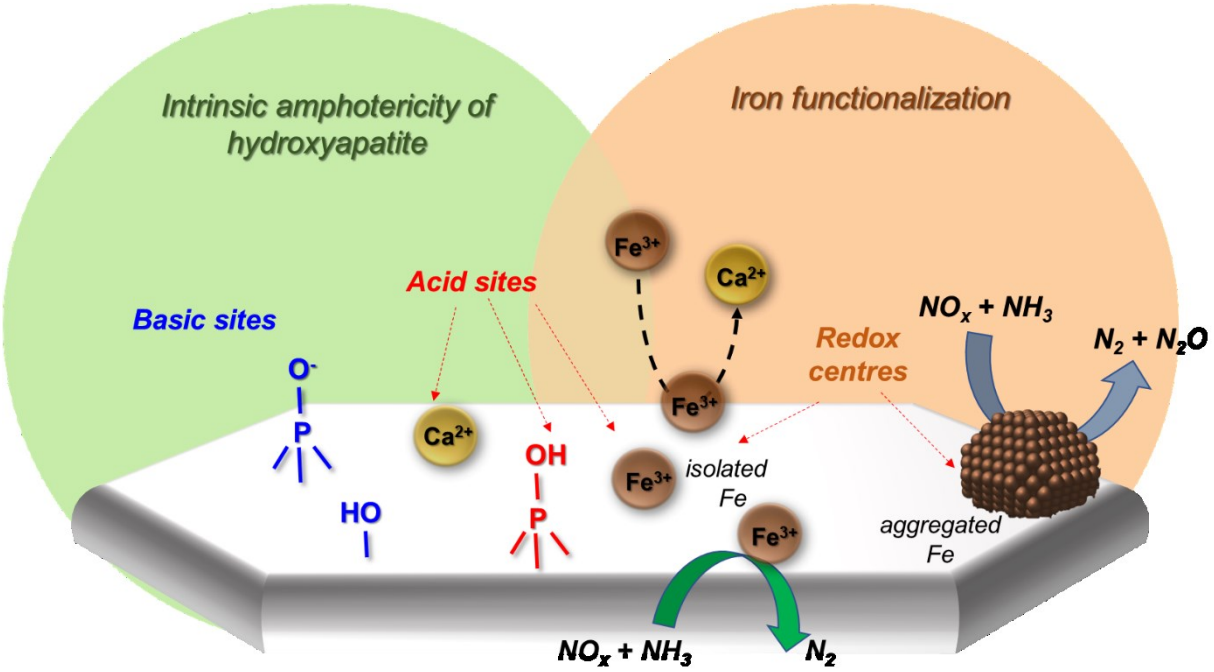

Table of Contents

Hydroxyapatite can be functionalised with iron thanks to the presence of exchangeable Ca sites. The intrinsic amphotericity of HAP together with the redox activity of iron centres make Fe/HAP samples promising NH_3-SCR catalysts. The exchanged isolated Fe centres showed high N_2 selectivity while aggregated α-Fe_2O_3/HAP promoted NH_3 overoxidation to N_2O.